10. Syrota A, Collard P, Paraf A. Comparison of ^{11}C-L-methionine uptake by the parotid gland and pancreas in chronic pancreatitis studied by positron emission tomography. *Gut* 1983;24:637–641.
11. Syrota A, Dop-Ngassa M, Cerf M, Paraf A. ^{11}C-L-methionine for evaluation of pancreatic exocrine function. *Gut* 1981;22:907–915.
12. Brown M, Marshall DR, Sobel BE, et al. Delineation of myocardial oxygen utilization with carbon-11 labeled acetate. *Circulation* 1987;76:687–696.
13. Buxton DB, Nienaber CA, Luxen A, et al. Noninvasive quantitation of regional myocardial oxygen consumption in vivo with [1-^{11}C] acetate and dynamic positron emission tomography. *Circulation* 1989;79:134–142.
14. Armbrecht JJ, Buxton DB, Brunken RC, Phelps ME, Schelbert HR. Regional myocardial oxygen consumption determined noninvasively in humans with [1-^{11}C] acetate and dynamic positron emission tomography. *Circulation* 1989;80:863–872.
15. Beanlands RSB, Bach DS, Raylman R, et al. Acute effects of dobutamine on myocardial oxygen consumption and cardiac efficiency measured using carbon-11 acetate kinetics in patients with dilated cardiomyopathy. *J Am Coll Cardiol* 1993;22: 1389–1398.
16. Calderon P, Furnelle J, Christophe J. In vitro lipid metabolism in the rat pancreas I: basal lipid metabolism. *Biochim Biophys Acta* 1979;574:379–390.
17. Shreve PD, Chiao P-C, Humes HD, Schwaiger M, Gross MD. Carbon-11-acetate PET imaging in renal disease. *J Nucl Med* 1995;36:1595–1601.
18. Pike VW, Eakins MN, Allan RM, Selwyn AP. Preparation of [1-^{11}C] acetate: an agent for the study of myocardial metabolism by positron emission tomography. *Int J Appl Radiat Isot* 1982;33:505–512.
19. Rösch J. Roentgenologic diagnosis of pancreatic disease. *Am J Roentgenol* 1967;100: 664–672.
20. Gorelick FS, Jamieson JD. Structure-function relationships of the pancreas. In: Johnson LR, ed. *Physiology of the Gastrointestinal Tract.* New York: Raven Press; 1981:773–794.
21. Hansson E. The formation of pancreatic juice proteins studied with labelled amino acids. *Acta Physiol Scand* 1959;46(suppl 161):3–99.
22. Comar D, Cartron JC, Maziere M, et al. Labelling and metabolism of methionine-methyl-^{11}C. *Eur J Nucl Med* 1976;1:11–14.
23. Zuidema GD, Kirsh M, Turcotte JG, Gaisford JG, Powers W, Kowalczyk RS. Pancreatic uptake of Se^{75}-selenomethionine. *Ann Surg* 1963;158:894–897.
24. Braganza J, Critchley M, Howat HT, et al. An evaluation of ^{75}Se selenomethionine scanning as a test of pancreatic function compared with the secritin-pancreozymin test. *Gut* 1973;14:383–389.
25. Bares R, Klever P, Hauptmann S, et al. F-18 fluorodeoxyglucose PET *in vivo* evaluation of pancreatic glucose metabolism for detection of pancreatic cancer. *Radiology* 1994;192:79–86.
26. Kato T, Fukatsu H, Ito K, et al. Fluorodeoxyglucose positron emission tomography in pancreatic cancer: an unsolved problem. *Eur J Nucl Med* 1995;22:32–39.
27. Inokuma T, Tamaki N, Torizuka T, et al. Value of fluorine-18-fluorodeoxyglucose and thallium-201 in the detection of pancreatic cancer. *J Nucl Med* 1995;36:229–235.
28. Friess H, Langhans J, Ebert M, et al. Diagnosis of pancreatic cancer by 2[^{18}F]-fluoro-2-deoxy-D-glucose positron emission tomography. *Gut* 1995;36:771–777.
29. Inokuma T, Tamaki N, Torizuka T, et al. Evaluation of pancreatic tumors with positron emission tomography and F-18 fluorodeoxyglucose: comparison with CT and US. *Radiology* 1995;195:345–352. Population

Technetium-99m-Labeled Chemotactic Peptides in Acute Infection and Sterile Inflammation

Conny J. van der Laken, Otto C. Boerman, Wim J.G. Oyen, Marjo T.P. van de Ven, D. Scott Edwards, John A. Barrett, Jos W.M. van der Meer and Frans H.M. Corstens

Departments of Nuclear Medicine and Internal Medicine, University Hospital Nijmegen, Nijmegen, The Netherlands; and Radiopharmaceuticals Division, The Du Pont Merck Pharmaceutical Company, North Billerica, Massachusetts

Chemotactic peptides have been proposed as vehicles to image infection and inflammation. Previous studies have shown high uptake at the site of infection soon after injection, most likely because of specific binding to receptors on locally present leukocytes. To investigate this hypothesis, the in vivo behavior of a synthetic chemotactic peptide was compared to a control peptide of similar molecular weight with low receptor binding affinity. In addition, the potential to target to different infections and sterile inflammation was tested. **Methods:** Twenty-four hours after induction of *Escherichia coli*, *Staphylococcus aureus* and zymosan abscesses, rabbits were i.v. injected with either 1 mCi of ^{99m}Tc-labeled formyl-methionyl-leucyl-phenylalanyl-lysine-hydrazinonicotinamide (^{99m}Tc-fMLFK-HYNIC) or ^{99m}Tc-labeled hydrazinonicotinamide-methionyl-leucyl-phenylalanyl-OMe (^{99m}Tc-HYNIC-MLFOMe, control peptide). Gamma camera images were obtained at 5 min and 1, 4, 8 and 20 hr postinjection. Biodistribution was determined at 20 hr postinjection. **Results:** The blood clearances of ^{99m}Tc-fMLFK-HYNIC and ^{99m}Tc-HYNIC-MLFOMe were similar. With time, ^{99m}Tc-fMLFK-HYNIC was retained in the abscess (*E. coli*), whereas the control agent ^{99m}Tc-HYNIC-MLFOMe was cleared from the abscess (0.049 ± 0.011 versus 0.005 ± 0.0003%ID/g at 20 hr postinjection; $p < 0.0005$). Abscess-to-contralateral muscle ratios of ^{99m}Tc-fMLFK-HYNIC rose to 36.8 ± 4.3 at 20 hr postinjection. *E. coli*, *S. aureus* and zymosan abscesses were clearly visualized from 4 hr postinjection onward. Abscess-to-background ratios increased to values varying from 4.4 ± 0.2 (zymosan) to 7.1 ± 0.6 (*S. aureus*) at 20 hr postinjection. The uptake in *S. aureus* and zymosan abscesses did not differ significantly from the uptake in *E. coli* abscesses. **Conclusion:** fMLFK-HYNIC is retained in both acute infection and sterile inflammation by means of specific receptor binding if sufficient cellular infiltration is present.

Key Words: chemotactic peptides; infection; inflammation; biodistribution; imaging

J Nucl Med 1997; 38:1310–1315

During the past few years, there has been a growing interest in the development of radiolabeled immunopeptides and proteins as radiopharmaceuticals for the imaging of infection and inflammation. Their small size and receptor binding capacity may make radiolabeled immunopeptides suitable agents for the rapid detection of inflammatory foci. The potential of several immunopeptides and proteins has already been demonstrated (*1–5*). One promising approach is the use of chemotactic peptides (*6*).

Chemotactic peptides, released by bacteria, cause leukocytes to marginate to nearby endothelial surfaces, move extravascularly and accumulate at sites where a chemotactin has been generated, a process called chemotaxis (*7*). Migration of cells from the blood to sites of tissue damage in the extravascular tissue is crucial to the development of inflammation. Schiffmann et al. (*8*) found that formyl peptides, synthetic analogs of natural bacterial products, were potent chemotactic factors for polymorphonuclear neutrophils (PMNs) and monocytes. These peptides initiate leukocyte chemotaxis by high-affinity binding to receptors present on both PMNs and mononuclear cells (*9,10*).

Fischman et al. (*1*) and Babich et al. (*2*) showed that acute infection in rats, rabbits and nonhuman primates can be clearly

Received Oct. 4, 1996; revision accepted Feb. 19, 1997.

For correspondence or reprints contact: Conny J. van der Laken, MD, Department of Nuclear Medicine, University Hospital Nijmegen, P.O. Box 9101, 6500 HB Nijmegen, The Netherlands.

visualized by ^{111}In- and ^{99m}Tc-labeled synthetic chemotactic peptides. Imaging of acute infection in rabbits with ^{99m}Tc-labeled chemotactic peptides was superior to ^{111}In-labeled white blood cells. High target-to-background ratios were obtained, probably as a result of accumulation of the chemotactic peptide at the site of infection.

Until now, increasing target-to-background ratios were assumed to be due to specific receptor binding of chemotactic peptides to leukocytes in inflammatory tissue, with concomitant clearance from the blood pool and other noninflamed tissues. These assumptions were based on correlations found between in vitro receptor binding and accumulation of the peptides at the site of inflammation in vivo. In this study, the specificity of focal uptake was studied directly in vivo. The in vivo behavior of the chemotactic peptide N-formyl-methionyl-leucyl-phenylalanyl-lysine (fMLFK) was compared to the behavior of a size-matched control peptide with low receptor binding affinity. Furthermore, the potential of the chemotactic peptide to localize in different acute infections as well as in sterile inflammation was explored.

MATERIALS AND METHODS

Peptide Synthesis

fMLFK was synthesized and purified as described by Fischman et al. (*1*) and conjugated to hydrazinonicotinic acid (HYNIC) as described by Babich et al. (*11*).

The peptide methionyl-leucyl-phenylalanyl-OMe (MLFOMe) was analogously synthesized and purified. HYNIC was conjugated to the N-terminal amine group of methionine. The peptide was used as control peptide in imaging and biodistribution studies.

Technetium-99m Labeling of HYNIC-Conjugated fMLFK and MLFOMe

In a 8-ml glass vial, 0.25 ml of 160 mg/ml tricine (in water), 100 μl of 0.05 mg/ml fMLFK-HYNIC or HYNIC-MLFOMe (in DMSO), 0.5 ml of 50–70 mCi $^{99m}TcO_4^-$ (in saline), 220 μl of ethanol and 30 μl of 1 mg/ml stannous chloride in 0.1 *N* HCl were mixed and incubated at room temperature for 0.5–1 hr. Subsequently, 400 μl of the reaction mixture was purified by reversed-phase chromatography using a 4.6 mm × 25 cm Zorbax Rx-C18 column. The following elution conditions were used: solvent A, 90% 25 m*M* sodium phosphate (pH 8) and 10% acetonitrile; solvent B, 50% 25 m*M* sodium phosphate (pH 8) and 50% acetonitrile; gradient, 0–100% solvent B over 25 min; flow rate, 1.0 ml/min; and UV absorption, 280 nm. The void fractions were collected in plastic tubes containing tricine (20–30 mg per tube) and transferred to a 25-ml round-bottomed flask. The solution was evaporated to dryness and then reconstituted with saline to proper concentrations for animal studies.

The radiochemical purity of the radiopharmaceuticals was determined by reversed-phase chromatography with the above described elution conditions and instant thin-layer chromatography on paper Whatman no. 1 strips with acetone and acetone:saline (3:1) as solvents.

Receptor Binding Assays

Human PMNs were isolated from heparinized venous blood obtained from healthy donors. Blood samples of 40 ml were mixed with an equal volume of Hanks' balanced salt solution (HBSS), layered on a Ficoll–Hypaque gradient and centrifuged at 10°C and 1300 rpm for 30 min. The supernatant was discarded, and the PMN-rich pellet was resuspended in cold HBSS, to which cold 2% dextran solution (in saline) was added to remove the contaminating red blood cells. After 25 min of sedimentation at room temperature, the suspended cells were removed and centrifuged at 10°C and 1300 rpm for 10 min. The supernatant was discarded, and the pellet was resuspended in 10 ml of cold hypotonic lysing buffer for a 5-min lysis of residual RBCs. After lysis, cold HBSS (40 ml) was added, and the cells were centrifuged at 10°C and 1300 rpm for 10 min. This final PMN pellet was washed once and resuspended to the desired cell concentration in phosphate buffered incubation buffer containing 140 m*M* NaCl, 1.0 m*M* KH_2PO_4, 5 m*M* Na_2HPO_4, 0.5 m*M* $MgCl_2$, 0.15 m*M* $CaCl_2$ and 0.5% BSA (pH 7.4) for fMLF binding assays. For the cytochrome C reduction assays, cells were resuspended in HBSS.

fMLF Binding Assay. [^{3}H]fMLF (10 n*M*), fMLFK-HYNIC or HYNIC-MLFOMe and 100 μl of PMN solution (8 × 10^6 PMNs/ml) were added to a 96-well microplate with filters (0.65-μm pore size). The microplate was incubated for 60 min at room temperature with gentle agitation. The microplate was then placed on a filtration system. The wells were washed with incubation buffer three times and dried. The filters were removed from the microplate, placed into scintillation vials and agitated for 1 hr at room temperature in the presence of scintillation fluid. Percent inhibition of [^{3}H]fMLF binding to PMNs was calculated by dividing the specific binding (total binding − nonspecific binding) obtained in the presence of fMLFK-HYNIC or HYNIC-MLFOMe by that obtained in the absence of these peptides. IC_{50} values were calculated by fitting the percent inhibition values to a regression line.

Cytochrome c PMN Free Radical Release Assay. The biologic activity of fMLFK-HYNIC was determined by measuring superoxide release of PMNs after they were exposed to fMLFK-HYNIC. Typically, PMN solution (1 ml, 1 × 10^6 PMNs/ml) was incubated with cytochalasin B (10 μ*M*) and 100 μl of cytochrome c (40 μ*M*) for 10 min at 37°C. Then, fMLFK-HYNIC was added, and tubes were incubated for 10 min at room temperature. After centrifugation (200 × g, 10°C for 10 min), the supernatants were transferred to cuvettes for spectrophotometric analysis to measure reduction of cytochrome c, reflecting the amount of superoxide release by PMNs. The percent of fMLFK-HYNIC response was determined. EC_{50} values were derived from concentration-response curves.

Animal Studies

Comparison of Technetium-99m-fMLFK-HYNIC and Technetium-99m-HYNIC-MLFOMe. Abscesses were induced in the left thigh muscle of female New Zealand rabbits weighing 2.2–2.8 kg with 1.5 × 10^{10} colony forming units of *Escherichia coli* in 0.5 ml. During the procedure, the rabbits were anesthetized with a subcutaneous injection of a 0.6-ml mixture of 0.315 mg/ml fentanyl and 10 mg/ml fluanisone. After 24 hr, when swelling of the muscle was apparent, groups of four rabbits were immobilized, placed prone on the gamma camera and injected with either 0.6 ml of 37 MBq ^{99m}Tc-fMLFK-HYNIC or 0.6 ml of 37 MBq ^{99m}Tc-HYNIC-MLFOMe in the lateral ear vein.

Images were recorded at 5 min and 1, 4, 8 and 20 hr postinjection with a single-head gamma camera equipped with a parallel-hole low-energy collimator. Images were obtained with a 75% symmetrical window over the 140-keV ^{99m}Tc energy peak. After acquisition of 50,000–100,000 counts, the images were digitally stored in a 256 × 256 matrix.

The scintigraphic results were analyzed quantitatively by drawing regions of interest over the abscess, the uninfected contralateral thigh muscle (background) and the whole body. Abscess-to-background ratios and percentage residual activity in the abscess (abscess-to-whole body ratio × 100%) were calculated.

After completion of the final images, rabbits were killed with a lethal dose of sodium phenobarbital. Samples of blood, infected thigh muscle, uninfected contralateral thigh muscle, bone, bone marrow, lung, spleen, liver, kidneys and intestines were collected. The dissected tissues were weighed and counted in the gamma

counter. To correct for radioactive decay, injection standards were counted simultaneously. The measured activity in samples was expressed as %ID/g. Abscess-to-contralateral muscle ratios and abscess-to-blood ratios were calculated.

The blood clearance of both labeled peptides was determined in groups of three rabbits with intramuscular *E. coli* infections per peptide. Blood samples were collected at 1, 5, 10, 20, 30, 60, 120 and 240 min after injection of the radiopharmaceuticals. The samples were weighed, measured and expressed as %ID/g.

In addition, white blood cell counts were measured in blood samples of healthy rabbits after injection of an equal amount of ^{99m}Tc-fMLFK-HYNIC as used in imaging and biodistribution studies. Blood samples were obtained at 1, 3, 5, 10, 30 and 60 min after injection.

Technetium-99m-fMLFK-HYNIC in Staphylococcus aureus- and Zymosan-Induced Inflammations. S. aureus abscesses were induced in the left thigh muscle of four rabbits as described above, with 5×10^8 bacteria in 0.5 ml. Sterile inflammations were similarly induced in four rabbits by intramuscular injection of 1 ml of 7.5% zymosan in sterile saline. Twenty-four hours after induction of the abscesses, rabbits were i.v. injected with 0.6 ml of 37 MBq ^{99m}Tc-fMLFK-HYNIC. The gamma camera imaging and determination of tissue biodistribution were performed as described above.

Statistical Analysis

All values are expressed as mean ± s.e.m. Statistical analysis was performed using a one-way ANOVA.

RESULTS

Radiolabeling and Characterization of the Technetium-99m-Labeled Peptides

Technetium-99m-fMLFK-HYNIC was eluted from the column in two overlapping peaks at 11–14 min. The control peptide, ^{99m}Tc-HYNIC-MLFOMe, was eluted from the column with a similar pattern at 18–21 min. The elution pattern showed a small additional peak at 6 min, presumably representing TcO_4^-, which was typically less than 10%. Reversed-phase chromatography analysis of the injected preparations did not show degradation. The radiochemical purity of both radiopharmaceuticals was >96%.

The binding of [^{3}H]fMLF to receptors on PMNs could be completely inhibited by fMLFK-HYNIC. The IC_{50} value of fMLFK-HYNIC was 3 ± 2 n*M*. Nonspecific binding on average was less than 15%. In contrast, HYNIC-MLFOMe did not show any inhibition at 100 n*M*. Furthermore, fMLFK-HYNIC was an effective inducer of superoxide release of PMN, with an EC_{50} value 0.8 ± 0.4 n*M*.

Animal Studies

Comparison of Technetium-99m-fMLFK-HYNIC and Technetium-99m-HYNIC-MLFOMe in E. coli Infections. After injection of ^{99m}Tc-fMLFK-HYNIC in healthy rabbits, a minimal transient reduction in peripheral leukocyte levels of short duration was observed: immediately after injection, the white blood cell count decreased to 65% of the initial level and returned to 90%–95% within 3 min after injection (Fig. 1). The same pattern was observed in infected rabbits (data not shown).

Technetium-99m-fMLFK-HYNIC and the control peptide, ^{99m}Tc-HYNIC-MLFOMe, rapidly cleared from the blood in a similar fashion (Fig. 2). After a fast initial biodistribution, ^{99m}Tc-fMLFK-HYNIC and ^{99m}Tc-HYNIC-MLFOMe cleared with t½ values of 16.4 ± 1.4 min and 13.4 ± 0.5 min, respectively, within the first hour and thereafter with t½ values of 203.2 ± 21.3 min and 301.4 ± 24.7 min, respectively.

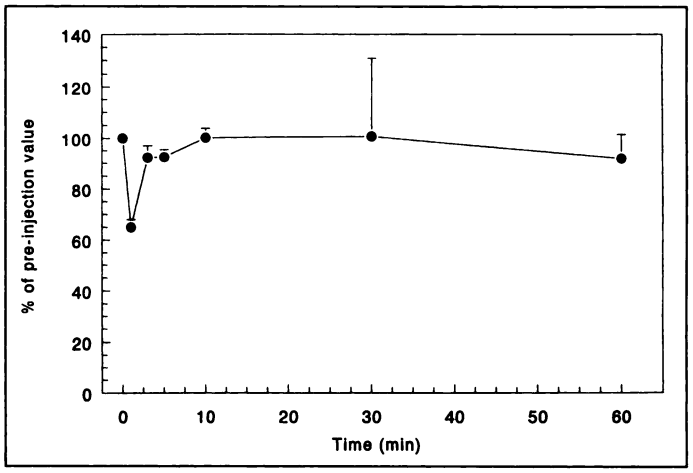

FIGURE 1. White blood cell counts in blood of healthy rabbits after injection of ^{99m}Tc-fMLFK-HYNIC, expressed as percentage of the preinjection value. Error bars, s.e.m.

Although ^{99m}Tc-fMLFK-HYNIC rapidly cleared from circulation, the images clearly showed rapid accumulation in the abscess (Fig. 3). The abscesses could already be visualized at 4 hr postinjection. With time, increased abscess uptake was visible, resulting in clearly delineated abscesses at 20 hr postinjection. In contrast, the control peptide ^{99m}Tc-HYNIC-MLFOMe cleared from the abscess during the time course of the study. In addition, the images showed high uptake of ^{99m}Tc-fMLFK-HYNIC in spleen, liver, kidneys and bladder. Uptake in the lungs was high immediately after injection but rapidly decreased with time. The control peptide, ^{99m}Tc-HYNIC-MLFOMe, showed marked accumulation in gallbladder and bowel.

The percentage residual activity of ^{99m}Tc-fMLFK-HYNIC in the abscess, derived from quantitative scintigrapic analysis, increased from 1.2% ± 0.1% at 5 min postinjection to 4.3% ± 0.2% at 20 hr postinjection, whereas the residual activity in the abscess of the control peptide ^{99m}Tc-HYNIC-MLFOMe decreased with time: from 2.0% ± 0.1% at 5 min postinjection to 0.5% ± 0.03% at 20 hr postinjection (Fig. 4). The abscess uptake of ^{99m}Tc-fMLFK-HYNIC was significantly higher from 1 hr postinjection onward ($p < 0.005$).

As a result of the increased uptake of ^{99m}Tc-fMLFK-HYNIC in the abscess and clearance of the background in the course of time, the abscess-to-background ratios continuously increased from 1.0 ± 0.04 at 5 min postinjection to 5.8 ± 0.9 at 20 hr postinjection (Fig. 5). Unlike the increasing ratios of ^{99m}Tc-

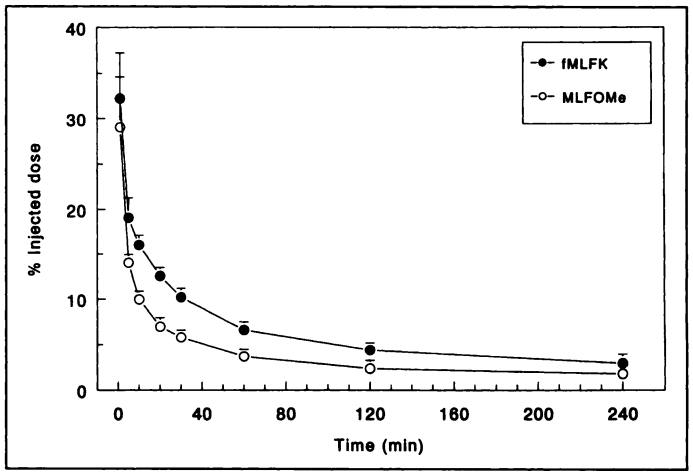

FIGURE 2. Blood clearance of ^{99m}Tc-fMLFK-HYNIC and ^{99m}Tc-HYNIC-MLFOMe determined in rabbits with *E. coli* infection. Data are expressed as percentage of the injected dose. Error bars, s.e.m.

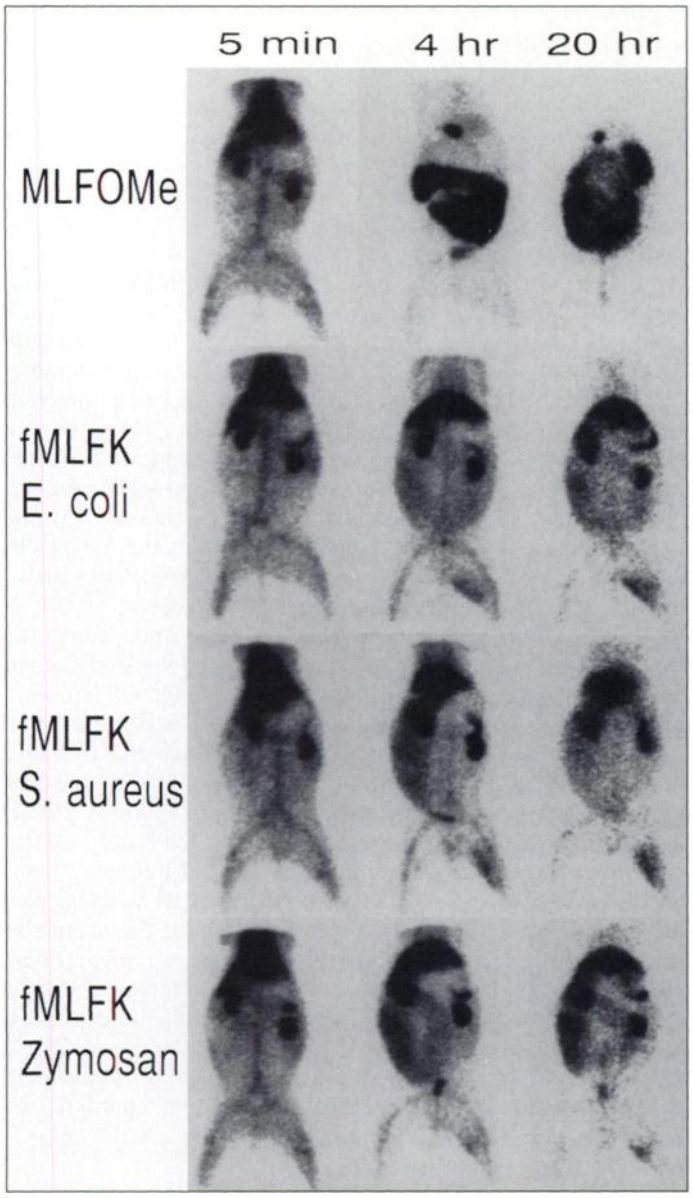

FIGURE 3. Images of rabbits with an *E. coli*-, *S. aureus*- or zymosan-induced abscess in the left thigh muscle at 5 min and 4 and 20 hr after injection of either ^{99m}Tc-fMLFK-HYNIC or ^{99m}Tc-HYNIC-MLFOMe (*E. coli* only). All photographs were produced with the same image contrast.

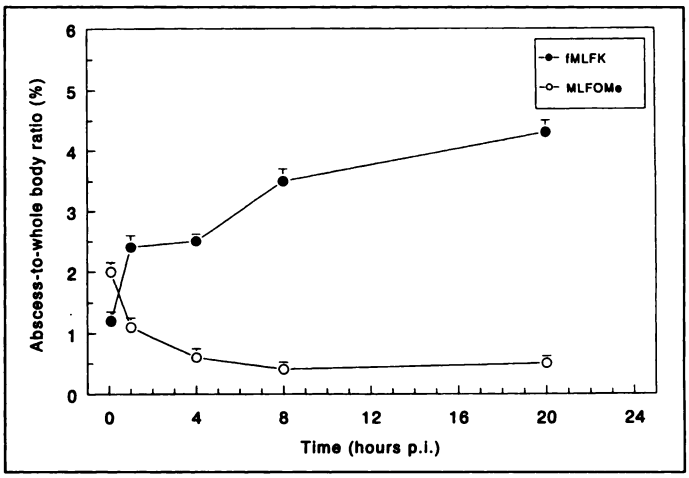

FIGURE 4. The percentage residual activity (abscess-to-whole body ratio × 100%) in rabbits with an *E. coli* infection injected with either ^{99m}Tc-fMLFK-HYNIC or ^{99m}Tc-HYNIC-MLFOMe. Error bars, s.e.m.

fMLFK-HYNIC, the ratios of ^{99m}Tc-HYNIC-MLFOMe reached the maximum value of 1.8 ± 0.1 at 1 hr postinjection and decreased thereafter to 1.2 ± 0.1 at 20 hr postinjection. From 4 hr postinjection onwards, the ratios of ^{99m}Tc-fMLFK-HYNIC were significantly higher than the ratios of ^{99m}Tc-HYNIC-MLFOMe ($p < 0.05$).

As determined by tissue biodistribution at 20 hr postinjection (Table 1), the abscess uptake of ^{99m}Tc-fMLFK-HYNIC was significantly higher than the uptake of ^{99m}Tc-HYNIC-MLFOMe, i.e., 0.049% ± 0.011%ID/g versus 0.005 ± 0.0003%ID/g ($p < 0.0005$). Due to rapid clearance of ^{99m}Tc-fMLFK-HYNIC from the contralateral muscle and retention in the abscess, the abscess-to-contralateral muscle ratios reached values of 36.8 ± 4.3 at 20 hr postinjection. The ratios of the control peptide, ^{99m}Tc-HYNIC-MLFOMe, were significantly lower: 6.0 ± 0.8 at 20 hr postinjection ($p < 0.0005$). Likewise, the abscess-to-blood ratios of ^{99m}Tc-fMLFK-HYNIC of 8.6 ± 0.9 were significantly higher than of ^{99m}Tc-HYNIC-MLFOMe of 1.0 ± 0.03 ($p < 0.0001$) (Fig. 6). The values for the uptake of ^{99m}Tc-fMLFK-HYNIC in lung ($p < 0.01$), bone marrow ($p < 0.005$), spleen ($p < 0.001$), liver ($p < 0.0001$) and kidney ($p < 0.0001$) were significantly higher than those of the control peptide. In contrast, the accumulation of ^{99m}Tc-HYNIC-MLFOMe in the feces was significantly higher ($p < 0.005$).

Comparison of Technetium-99m-fMLFK-HYNIC in E. coli-, S. aureus- and Zymosan-Induced Inflammations. The images in Figure 3 demonstrate that *E. coli*- and *S. aureus*-induced infections and sterile inflammations induced by zymosan were all clearly visualized by ^{99m}Tc-fMLFK-HYNIC. Quantitative analysis of the scintigraphic data showed increasing abscess-to-background ratios in all three models to values varying from 4.4 ± 0.2 (zymosan) to 7.1 ± 0.6 (*S. aureus*) at 20 hr postinjection (Fig. 5).

Tissue biodistribution data, summarized in Table 1, were in agreement with the imaging data. Biodistributions of ^{99m}Tc-fMLFK-HYNIC in the three models were similar. There were no significant differences in uptake in *S. aureus*-, *E.coli*- or zymosan-induced inflammations. Both the abscess-to-contralateral muscle ratios and the abscess-to-blood ratios in the *S. aureus* and the zymosan models were as high as the ratios obtained in the *E. coli* model (Fig. 6). The sterility of the zymosan-induced inflammations was confirmed by microbiologic examination.

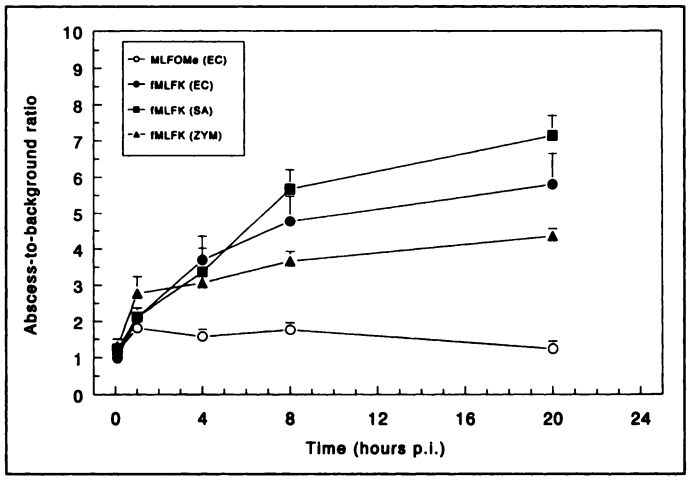

FIGURE 5. The abscess-to-background ratios in rabbits with an *E. coli* (EC)-, *S. aureus* (SA)- or zymosan (ZYM)-induced abscess, injected with ^{99m}Tc-fMLFK-HYNIC or ^{99m}Tc-HYNIC-MLFOMe (*E. coli* only). Error bars, s.e.m.

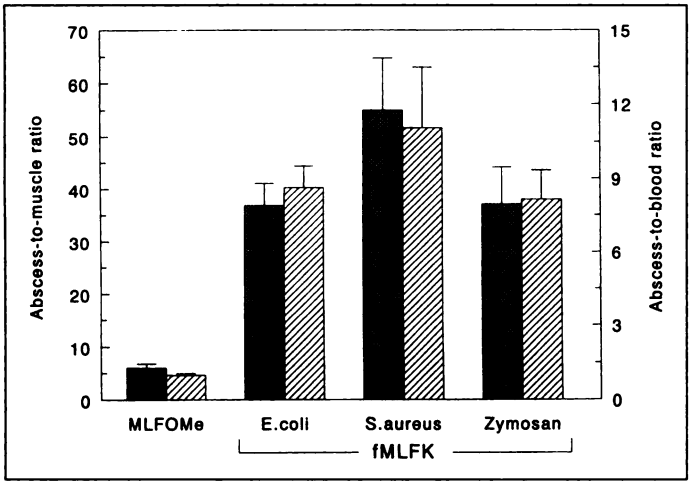

FIGURE 6. Abscess-to-contralateral muscle ratios (■) and abscess-to-blood ratios (▨), calculated from rabbits with an *E. coli*-, *S. aureus*- or zymosan-induced abscess, injected with ^{99m}Tc-fMLFK-HYNIC or ^{99m}Tc-HYNIC-MLFOMe (*E. coli* only). Error bars, s.e.m.

DISCUSSION

Our results indicate that accumulation of fMLFK-HYNIC in acute infection and sterile inflammation takes place by virtue of binding to receptors on locally present PMNs and monocytes. The studied chemotactic peptide fMLFK-HYNIC was retained in infection, whereas a size-matched control peptide with low receptor binding affinity cleared from the infection with time.

To study the hypothesis of specific retention of fMLFK-HYNIC in infection and inflammation, we searched for a control agent with the most favorable characteristics for this purpose. HYNIC-MLFOMe met the requirements because it was a similar-sized peptide that highly resembled fMLFK-HYNIC and had a significantly lower affinity for receptors on PMNs and monocytes. Because it was more hydrophobic than fMLFK-HYNIC, a different route of clearance was observed. As shown by the scintigraphic data as well as by tissue biodistribution, fMLFK-HYNIC was cleared via both the kidneys and liver. Hepatobiliary clearance was the main route of clearance of HYNIC-MLFOMe. As a result, high activity uptake in liver, gallbladder and bowel was visible. Despite different routes of clearance, blood clearances of the two peptides was similar. Therefore, localization in infection could be compared. The different behavior of fMLFK-HYNIC compared to HYNIC-MLFOMe in terms of uptake of fMLFK-HYNIC in the abscess and clearance of HYNIC-MLFOMe from the abscess could be attributed to differences in receptor binding. The binding of fMLFK-HYNIC to receptors on leukocytes is furthermore reflected in high uptake of the agent in spleen and liver. In addition, the observation that ^{99m}Tc-tricine did not accumulate in infection provided further evidence of specific receptor binding of fMLFK-HYNIC in inflammatory tissue (data not shown). These data are in line with data reported by Babich et al. (*12*). They found a correlation between the infection localization properties of chemotactic peptides in vivo and the fMLF receptor affinity, as determined in vitro. Nonspecific accumulation did not contribute significantly to infection localization.

Our data demonstrated that fMLFK-HYNIC localizes in both infection and sterile inflammation. These findings contradict results obtained by Fischman et al. They reported infection selective localization of chemotactic peptides, based on the observation that low levels of peptide were found in uninfected thermally injured tissues in rabbits (*13,14*) and sterile inflammations induced by intramuscular injection of anesthetic agents in nonhuman primates (*15*). However, assuming that the mechanism of localization of chemotactic peptides at sites of inflammation takes place by virtue of binding to receptors on PMNs and monocytes, it is to be expected that infiltration of significant numbers of these cells in tissue damaged by a sterile agent can be visualized with labeled chemotactic peptides. Therefore, most likely, accumulation of chemotactic peptide was not found in the described sterile lesions used by Fischman et al. because of a lack of cellular infiltration. This would be in agreement with low accumulation of peptide in turpentine induced inflammatory foci (data not shown), which are characterized by significant increased vascular permeability but minimal granulocyte infiltration (*16,17*). Apparently, increased vascular permeability only does not result in localization of the peptide at the site of the lesion. Other data support these suggestions: chemotactic peptides accumulate in chronic intestinal inflammation in rats and in lungs of rats with infiltration of neutrophils as a result of severe trauma (*18,19*). In accordance with these reports, our results demonstrate accumulation of chemotactic peptide in zymosan-induced sterile inflammation, an inflammation characterized by infiltration of PMNs and monocytes (*20,21*).

The slightly lower uptake of fMLFK-HYNIC in the zymosan-induced sterile inflammation compared to the uptake in *E. coli*- and *S. aureus*-induced infections could be explained by differences in severity of the inflammation. Injection of *E. coli* and *S. aureus* induced more severe inflammation than could be obtained by injection of zymosan. In fact, the severity of the infection can be increased by injection of more bacteria. Babich

TABLE 1
Biodistribution of Technetium-99m-fMLFK-HYNIC in the *E. coli*, *S. aureus* and Zymosan Models and of Technetium-99m-HYNIC-MLFOMe in the *E. coli* Model at 20 hr Postinjection (%ID/g, Mean Values ± s.e.m.)

	E. coli			
Organ	HYNIC-MLFOMe	fMLFK-HYNIC	*S. aureus*	Zymosan
Blood	0.005 ± 0.001	0.005 ± 0.0003	0.005 ± 0.001	0.004 ± 0.001
Abscess	0.005 ± 0.0003	0.049 ± 0.011	0.056 ± 0.012	0.035 ± 0.007
Muscle	0.001 ± 0.0004	0.001 ± 0.0003	0.001 ± 0.0003	0.001 ± 0.0002
Bone	0.002 ± 0.001	0.007 ± 0.005	0.01 ± 0.002	0.006 ± 0.005
Marrow	0.002 ± 0.001	0.036 ± 0.013	0.047 ± 0.009	0.050 ± 0.026
Lung	0.003 ± 0.0003	0.025 ± 0.010	0.048 ± 0.024	0.015 ± 0.004
Spleen	0.003 ± 0.001	0.430 ± 0.111	0.501 ± 0.231	0.327 ± 0.066
Kidney	0.020 ± 0.004	0.145 ± 0.014	0.138 ± 0.021	0.163 ± 0.030
Liver	0.013 ± 0.005	0.094 ± 0.017	0.114 ± 0.007	0.067 ± 0.011
Intestine	0.073 ± 0.057	0.033 ± 0.014	0.052 ± 0.041	0.088 ± 0.050
Feces	0.196 ± 0.065	0.028 ± 0.011	0.052 ± 0.025	0.016 ± 0.013

et al. (*2*) obtained higher uptake values of fMLFK-HYNIC in *E. coli* abscesses with 1×10^{11} bacteria than we reported for similar abscesses by injection of 1.5×10^{10} bacteria. We could not inject more *E. coli* because we used the maximum obtainable *E. coli* concentration. *S. aureus* was more pathogenic; less bacteria (5×10^8) induced more severe infections compared to *E. coli*, resulting in even higher uptake in *S. aureus* infections. Concentrations of *S. aureus* of 5×10^9 bacteria/ml were lethal. For induction of the sterile inflammations, we used the maximum obtainable concentration of zymosan, which was as high as 7.5%.

The specific activity of the injected preparation could not be determined because the diluted concentrations of fMLFK-HYNIC used did not have appreciable UV absorbance at 280 nm. However, in vivo, the induced transient neutropenia appeared to be minimal and of short duration, indicating that excess of unlabeled fMLFK-HYNIC had been removed by reversed-phase chromatography and that minimal amounts of fMLFK-HYNIC were injected in the rabbits. A study in nonhuman primates (*22*) showed that a similar minimal decrease in white blood cell count of short duration was observed when a dose as low as 10 ng/kg of chemotactic peptide was injected.

It has been shown that the nature of the coligand has effects on the biodistribution of ^{99m}Tc-labeled HYNIC-derivatized chemotactic peptides (*23*). Most previous studies with these peptides have used glucoheptonate as coligand for the radiolabeling. Nevertheless, tricine was selected for our studies because, in the same animal model, higher abscess uptake as well as higher abscess-to-background ratios were obtained with tricine compared to glucoheptonate (data not shown).

CONCLUSION

Both acute infection and sterile inflammation can be specifically targeted with radiolabeled chemotactic peptides, provided that these lesions are characterized by sufficient infiltration of PMNs and monocytes. Therefore, in principal, distinction between infection and inflammation cannot be made. The lesions could be visualized as early as 4 hr after injection. High focal uptake was obtained. More studies are required to evaluate whether chemotactic peptides are suitable agents for detection of chronic inflammatory diseases because most tested models thus far concerned acute infection or inflammation.

Several in vivo characteristics of chemotactic peptides need to be optimized. Detection of lesions localized in liver, spleen, kidneys or even bowels, especially in the case of less severe lesions, will be difficult to detect with chemotactic peptides because of high physiologic uptake in these organs. Because this is a major limitation of almost every infection detection agent, possible ways to modify the peptides to decrease background activity in the abdomen should be explored. In addition, reduction of biologic activity of chemotactic peptides will be necessary to apply chemotactic peptides clinically. The development of a high specific activity ^{99m}Tc-labeling has been a step in the right direction but does not warrant safe administration to humans. Therefore, further research in this area should focus on the development of antagonists or biologically less active agonists with similar binding characteristics.

ACKNOWLEDGMENTS

We thank the research group of M. J. Abrams, PhD (Johnson Matthey Pharmaceutical Research, West Chester, PA), for the synthesis of the control peptide HYNIC-MLFOMe, D. Glowacka, MD and T.D. Harris, MD for analysis and purification of the peptides, P. Mast for determination of the leukocyte counts and G. Grutters and H. Eijkholt (University of Nijmegen, Central Animal Laboratory) for technical assistance.

REFERENCES

1. Fischman AJ, Pike MC, Kroon D, et al. Imaging focal sites of bacterial infection in rats with indium-111-labeled chemotactic peptide analogs. *J Nucl Med* 1991;32:483–491.
2. Babich JW, Graham W, Barrow SA, et al. Technetium-99m-labeled chemotactic peptides: comparison with indium-111-labeled white blood cells for localizing acute bacterial infection in the rabbit. *J Nucl Med* 1993;34:2176–2181.
3. van der Laken CJ, Boerman OC, Oyen WJG, et al. Specific targeting of infectious foci with radioiodinated human recombinant interleukin-1 in an experimental model. *Eur J Nucl Med* 1995;22:1249–1255.
4. Signore A, Chianelli M, Toscano A, et al. A radiopharmaceutical for imaging areas of lymphocytic infiltration: ^{123}I-interleukin-2. Labelling procedure and animal studies. *Nucl Med Commun* 1992;13:713–722.
5. Hay RV, Skinner RS, Newman OC, et al. Nuclear imaging of acute inflammatory lesions with recombinant human interleukin-8 [Abstract]. *J Nucl Med* 1993;34:104P.
6. Corstens FHM, van der Meer JWM. Chemotactic peptides: new locomotion for imaging of infection? *J Nucl Med* 1991;32:491–494.
7. Ward PA, Lepow IH, Newman LJ. Bacterial factors chemotactic for polymorphonuclear leukocytes. *Am J Pathol* 1968;52:725–736.
8. Schiffmann E, Corcoran BA, Wahl SM. N-formylmethionyl peptides as chemoattractants for leukocytes. *Proc Natl Acad Sci USA* 1975;72:1059–1062.
9. Niedel J, Wilkinson S, Cuatrecasas P. Receptor-mediated uptake and degradation of ^{125}I-chemotactic peptide by human neutrophils. *J Biol Chem* 1979;254:10700–10706.
10. Williams LT, Snyderman R, Pike MC, Lefkowitz RJ. Specific receptor sites for chemotactic peptides on human polymorphonuclear leukocytes. *Proc Natl Acad Sci USA* 1977;74:1204–1208.
11. Babich JW, Solomon H, Pike MC, et al. Technetium-99m-labeled hydrazino nicotinamide derivatized chemotactic peptide analogs for imaging focal sites of bacterial infection. *J Nucl Med* 1993;34:1964–1974.
12. Babich JW, Higgins JD, Abrams MJ, et al. Infection imaging with radiolabeled chemotactic peptides: relationship between receptor affinity and infection [Abstract]. *J Nucl Med* 1994;35:44P.
13. Fischman AJ, Babich JW, Barrow SA, et al. Detection of acute bacterial infection within soft tissue injuries using a ^{99m}Tc-labeled chemotactic peptide. *J Trauma* 1995;38:223–227.
14. Fischman AJ, Babich JW, Rubin RH. Infection imaging with technetium-99m-labeled chemotactic peptide analogs. *Semin Nucl Med* 1994;24:154–168.
15. Fischman AJ, Babich JW, Barrow SA, Rubin RH. Detection of focal infection in non-human primates with a Tc-99m-labeled chemotactic peptide [Abstract]. *J Nucl Med* 1995;36:205P.
16. Vegad JL, Lancaster MC. Histological study of increased vascular permeability in the sheep in turpentine-induced inflammation of skin and pleura. *Indian J Exp Biol* 1973;11:494–497.
17. Svanes K. Diphasic increase of vascular permeability in turpentine-induced inflammation in skin and musculature of mice. *Acta Pathol Microbiol Scand A* 1971;79:335–344.
18. Carter EA, Tompkins RG, Babich JW, Fischman AJ. Accumulation of Tc-99m chemotactic peptides in chronic intestinal inflammation [Abstract]. *J Nucl Med* 1996;37:239P.
19. Carter EA, Tompkins RG, Babich JW, Fischman AJ. Severe trauma increases Tc-99m chemotactic peptide accumulation in lung: comparison with In-111 WBCs [Abstract]. *J Nucl Med* 1996;37:240P.
20. Lefkowitz JB. Essential fatty acid deficiency inhibits the in vivo generation of leukotriene B4 and suppresses levels of resident and elicited leukocytes in acute inflammation. *J Immunol* 1988;140:228–233.
21. Dawson J, Sedgewick AD, Edwards JC, Lees P. A comparative study of the cellular, exudative and histological responses to carrageenan, dextran and zymosan in the mouse. *Int J Tissue React* 1991;13:171–185.
22. Fischman AJ, Rauh D, Solomon H, et al. In vivo bioactivity and biodistribution of chemotactic peptide analogs in nonhuman primates. *J Nucl Med* 1993;34:2130–2134.
23. Babich JW, Fischman AJ. Effect of "co-ligand" on the biodistribution of ^{99m}Tc-labeled hydrazino nicotinic acid derivatized chemotactic peptides. *Nucl Med Biol* 1995;22:25–30.